

Optimizing the Proton Conductivity with the Isokinetic Temperature in Perovskite-Type Proton Conductors According to Meyer–Neldel Rule

Peng Du, Nana Li, Xiao Ling, Zhijun Fan, Artur Braun, Wenge Yang,* Qianli Chen,* and Arthur Yelon

Perovskite-type metal oxides such as Y-doped BaMO₃ (M = Zr/Ce) have drawn considerable attention as proton-conducting electrolytes for intermediate temperature ceramic electrochemical cells. Improving the proton conductivity at lower temperatures requires a comprehensive understanding of the proton conduction mechanism. By applying high pressure or varying the Ce content of Y-doped BaMO₃, it is demonstrated that the proton conductivity follows the Meyer–Neldel rule (MNR) well. In the Arrhenius plot, the conductivities intersect at an isokinetic temperature, where the proton conductivity is independent of activation energy. Considering the relationship between isokinetic temperature and lattice vibration frequency, a high isokinetic temperature is observed in materials with stiff lattices, consisting of light atoms and small M–O bond length. Based on consideration of the MNR, it is suggested that the enhancement of proton conductivity at low temperature can be well achieved by tuning lattice vibration frequency toward a desired isokinetic temperature.

proton-conducting electrolytes for intermediate temperature (450–700 °C) proton-conducting ceramic fuel cells (IT-PCFCs).^[1–7] Fully understanding the proton transport mechanisms is vital for the improvement of proton conductivity. To form protonic defects, BaMO₃ is doped with trivalent elements to create oxygen vacancies. In a humid environment, water is incorporated to the oxygen vacancies so that the protonic defects are formed at interstitial sites.^[8–12] The protons migrate along oxygen sites in the ZrO₆ octahedra. Classically, this migration process is described by the Grotthuss (hopping) mechanism, involving proton reorientation around the oxygen and hopping to an adjacent oxygen site.^[1,13] Yamazaki et al. proposed that protons are trapped by oxygens around the trivalent dopants.^[10]

1. Introduction

Perovskite-type metal oxides, such as barium zirconate and cerate (BaMO₃ where M = Zr/Ce) are promising

Thermal activation drives the proton hopping from one oxygen to another oxygen nearby by overcoming an energy barrier.

The temperature-dependent proton conductivity, σ , follows the Arrhenius equation

$$\sigma T = \sigma_0 \exp\left(-\frac{E_a}{k_B T}\right) \quad (1)$$

where T is the temperature, σ_0 is an experimental prefactor, E_a is the activation energy, and k_B is the Boltzmann constant.

Since the discovery of ceramic proton conductors in the 1980s, there has been an ongoing quest to improve the proton conductivity at intermediate temperature. According to the Arrhenius equation, lowering the activation energy is considered as an effective approach. Nevertheless, it is widely observed^[14] that the Arrhenius prefactor and the activation energy show the following relationship, that affects the conductivity

$$\ln \sigma_0 = \ln \sigma_{00} + \frac{E_a}{k_B T_{\text{iso}}} \quad (2)$$


where σ_{00} and T_{iso} are constants, as further explained below. Equation (2) is known as Meyer–Neldel rule (MNR), a compensation law, as the change in prefactor compensates the change in activation energy.^[15,16] Prior to Meyer and Neldel,

P. Du, X. Ling, Z. Fan, Q. Chen
University of Michigan – Shanghai Jiao Tong University Joint Institute
Shanghai Jiao Tong University
Shanghai 200240, China
E-mail: qianli.chen@sjtu.edu.cn

N. Li, W. Yang
Center for High Pressure Science & Technology Advanced Research (HPSTAR)
Shanghai 201203, China
E-mail: yangwg@hpstar.ac.cn

A. Braun
Laboratory for High Performance Ceramics
Empa - Swiss Federal Laboratories for Materials Science and Technology
Dübendorf CH-8600, Switzerland

A. Yelon
Département de Génie Physique
Polytechnique Montréal
and Réseau Québécois sur des Matériaux de Pointe (RQMP)
CP 6079, Succursale C.-V.
Montréal QC H3C 3A7, Canada

 The ORCID identification number(s) for the author(s) of this article can be found under <https://doi.org/10.1002/aenm.202102939>.

DOI: 10.1002/aenm.202102939

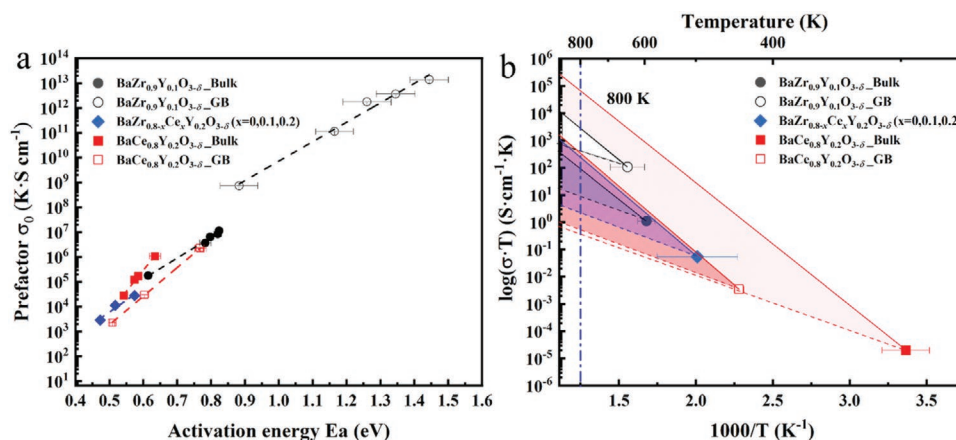


Figure 1. a) Correlation between Arrhenius prefactor σ_0 and activation energy E_a (MN plot) and b) the corresponding isokinetic temperature for BaZr_{0.9}Y_{0.1}O_{3- δ} ^[31,32] and BaCe_{0.8}Y_{0.2}O_{3- δ} ^[30] under high pressure for bulk and grain boundary (GB) conductivities, and for BaZr_{0.8-x}Ce_xY_{0.2}O_{3- δ} ($x=0, 0.1, 0.2$) bulk conductivities.^[33] Shaded areas represent the conductivity range when the activation energies vary between 0.4 eV (dotted lines) and 0.9 eV (solid lines), simulated according to Equation (4). The blue dashed-dotted line indicates the proton conductivity at 800 K.

Constable found a similar relation in data about the catalytic decomposition of organic molecules on metal surfaces.^[17] Such a compensation “law” has been discovered in many different fields and appears to be a universal statistical relationship.^[18] At T_{iso} , the conductivity is independent of activation energy. Therefore, the MNR is also called isokinetic rule and T_{iso} is known as the isokinetic temperature. The prefactor, σ_0 , is called the “isokinetic prefactor” in the following text. In general, Equation (2) has been observed^[19,20] in many fields and a wide range of kinetic phenomena, when the activation energy, E_a , is greater than the thermal energy $k_B T$ and phonon energies.

Yelon and co-workers proposed the multiexcitation entropy model^[14] to describe the high activation energy kinetics for high-temperature conductivity. This model pointed out that when E_a is large compared to the excitation energy or thermal energy, a fluctuation providing multiple excitation is necessary to overcome the energy barrier.

The isokinetic temperature is related to an excitation energy, $h\nu$, to which the charge carriers must couple, in order to overcome the activation barrier, expressed by^[14,20]

$$k_B T_{\text{iso}} = \frac{h\nu}{\ln \kappa} \quad (3)$$

where h is the Planck constant, ν is the excitation frequency, and κ is a coupling constant. As observed experimentally, $\ln \kappa$ is usually between 0.5 and 2. The excitations may involve phonons or local excitations.^[14]

The impact of phonons and lattice dynamics on ionic conductivity has drawn considerable attention in recent years.^[21–27] Previous studies have shown that a softer lattice leads to a lower activation barrier for ion migration.^[21,22,27–28] In lithium superionic conductors, Zeier and co-workers^[21] proposed that changes in polyhedral species lead to a variation in phonon modes. Shao-Horn and co-workers proposed to use the phonon band center as a descriptor for the average phonon frequency of mobile ion, and concluded that lowering the phonon band center can reduce the activation barrier for ion migration in lithium superionic conductors and olivine ion conductors.^[25,26]

We have found, for proton conducting barium zirconate^[22] and cerate,^[29,30] by applying high pressure, that low activation energy for proton conductivity is correlated to the softening of Raman modes. Particular modes of the phonons seem to propel the protons through the crystal lattice, following the quantitative description of a Holstein-type proton polaron.^[23,24]

Previous studies have demonstrated the importance of lattice dynamics on design of many fast ionic conductors. However, for proton conductors, it remains unclear how to tune the proton conductivity based on lattice dynamics. In the present work, we first show that the proton conductivity in perovskites follows the MNR. Then, based on the effect of pressure on BaZr_{0.9}Y_{0.1}O_{3- δ} (BZY), a model system, we consider the role of phonon excitation in proton conductivity. For further investigation of the proton–phonon coupling, we apply a controllable method of varying the proton conductivity, this is, introducing the external applied pressure as a thermodynamic variable and tunable technical parameter. This permits tuning of the crystal structure and vibrational frequency of the ZrO₆ octahedron without introducing potential microstructural changes due to material processing, which can happen in the case of chemical pressure by doping and substitution. After investigating the correlation between Raman modes and the proton conductivity in BZY under high pressure, we propose to use the average M–O stretch vibration, defined below, as a simple descriptor of lattice dynamics. Based on these results, a novel quantitative relationship between isokinetic temperature, vibrational frequency, and proton–phonon coupling is revealed.

2. Results

2.1. Proton Conductivity in Perovskites: An Investigation According to MNR

To verify whether MNR describes proton conductivity in the perovskite proton conductors, we plot the Arrhenius prefactor σ_0 versus the activation energy E_a – a Meyer–Neldel (MN) plot – for BZY and BaCe_{0.8}Y_{0.2}O_{3- δ} (BCY) measured under high

pressure,^[30–32] and BaZr_{0.8–x}Ce_xY_{0.2}O_{3–δ} ($x = 0, 0.1, \text{ and } 0.2$, denoted as BZCY) with varying Ce compositions at ambient pressure,^[33] as shown in **Figure 1a**. The detailed proton conductivity data for bulk and grain boundaries used to extract σ_0 and E_a are presented in Figure S1 (Supporting Information). Varying mechanical pressures (either on bulk material, as we have done, or by thin film epitaxy) and chemical compositions are two distinct approaches for modification of the material structure. Proton conductivity can be tuned accordingly. Typically, the activation energy for bulk proton conductivity can be changed between 0.4 and 0.9 eV using these approaches, as shown in Figure 1a. The relationship between prefactors and activation energies in Figure 1a agrees with Equation (2), validating the application of MNR to proton conductivity in BaMO₃ ($M = \text{Zr/Ce}$) when the material structure is changed using different approaches. This MN behavior can be explained by the local volume change in atomic structure associated with ion migration.^[34] The isokinetic temperatures T_{iso} can be obtained from the inverse slopes of the MN plots, according to Equation (2).

Combining Equations (1) and (2), the Arrhenius relationship can be written as

$$\sigma = \frac{\sigma_{00}}{T} e^{\left(\frac{-E_a}{k_B}\right) \left(\frac{1}{T} - \frac{1}{T_{\text{iso}}}\right)} \quad (4)$$

Equation (4) shows that, at T_{iso} , the proton conductivity has a single value.^[20] For $T \leq T_{\text{iso}}$, the highest values of σ are obtained for the lowest values of E_a . For $T \geq T_{\text{iso}}$, the highest σ corresponds to the largest E_a . Such behavior is observed only occasionally^[20] in studies of MNR, in all fields. This is due to the fact that, as T is increased, Equation (4) will eventually no longer describe the experimental observations, due to changes in the kinetic mechanism, changes in material structure, or, finally, to breakdown of the condition that E_a be larger than $k_B T$. This often happens before T_{iso} is reached. We have studied σ between room temperature and 800 K,^[30,31] and verified the application of Equation (4) in both regimes.

The calculated isokinetic temperatures are shown in an Arrhenius plot in Figure 1b. Notably, for the bulk conductivities, the T_{iso} for BZY is twice as high as that of BCY. The T_{iso} for grain boundary conductivities are higher than those of bulk conductivities. We show the range in which proton conductivity can be tuned (shaded area) assuming the activation energy varies from 0.4 eV (dotted lines) to 0.9 eV (solid lines) according to Equation (4). Note that this calculation shows the proton conductivities in an ideal case based on the MNR, e.g., assuming that the proton concentration is constant. Figure 1b shows that the T_{iso} of BCY is lower than that of BZY; however, the adjustable range for proton conductivity is the largest among all the three materials when changing the activation energy between 0.4 and 0.9 eV. Here, we face an interesting paradox: let us assume that the working temperature is 800 K, which is a realistic operation temperature for PCFCs. 800 K is higher than the isokinetic temperature in all reported cases here. As discussed above, it will then be necessary to increase the activation energy, counterintuitive to the general experience that activation energies should be lowered. Figure 1b reveals that materials with low T_{iso} , such as BCY, provide a large tunable range

for proton conductivity when the activation energy is changed within the same range. From Figure 1b and Equation (4), we can understand that in order to apply an appropriate strategy for tuning the activation energy, it is essential to determine T_{iso} . The importance of $k_B T_{\text{iso}}$ in guiding the search for new ionic conductor materials has been discussed in detail elsewhere.^[35]

2.2. Role of Phonons in Proton Transport

We have presented the importance of isokinetic temperature for the design of proton conducting perovskites. However, the effects of material structure and phonons on isokinetic temperature remain unclear. To find any causal relationship between material vibrational character and proton conductivity, we calculated the Meyer–Neldel energies $k_B T_{\text{iso}}$ for the reported isokinetic temperatures T_{iso} , and the corresponding range of excitation phonon energies $h\nu$ and wavenumbers $\bar{\nu}$, according to Equation (3) for the materials presented in Figure 1, as listed in **Table 1**. Here, we focus our discussion on the bulk conductivity, with the corresponding lattice vibration being primarily a bulk property. From the calculated results, we find that the excitation frequencies typically fall in the range of phonon vibrations. When Zr is substituted by Ce, T_{iso} decreases, accompanied by a reduction in excitation energy.

BaZrO₃ has a stiffer lattice than BaCeO₃. This is reflected in a much higher Raman shift in Zr–O stretch mode (750 cm⁻¹^[22]) than that in Ce–O stretch mode (350 cm⁻¹^[29]). The vibrational energies of these stretch modes are within the range of the calculated excitation, as shown in Table 1. Inspired by these findings, we further investigate the correlation between the excitation energy and phonon vibration.

We use Raman spectroscopy to investigate the variation of phonon vibration with the increase of pressure for BZY, as shown in Figure S2 (Supporting Information). The prominent characteristic bands vary significantly with pressure. According to the density functional theory study on BaZrO₃,^[11] the Raman bands at around 107, 231, and 458 cm⁻¹ correspond to Ba–ZrO₆ stretching, ZrO₆ torsion, and O–Zr–O bending motions, respectively. The two Raman bands at 600 and 750 cm⁻¹ represent the Zr–O stretching motion. In order to gain quantitative information on how the different Raman modes in BZY change with pressure, we fit the Raman spectra using Gaussian functions. As shown in **Figure 2**, three Gaussian peaks labeled as

Table 1. The isokinetic prefactor σ_{00} , isokinetic temperature T_{iso} , Meyer–Neldel energy $k_B T_{\text{iso}}$, excitation energy $h\nu$, and the corresponding phonon wavenumber $\bar{\nu}$ for BaZr_{0.9}Y_{0.1}O_{3–δ}, BaZr_{0.8–x}Ce_xY_{0.2}O_{3–δ} ($x = 0, 0.1, 0.2$), and BaCe_{0.8}Y_{0.2}O_{3–δ}. The excitation energy was calculated according to Equation (3) assuming the coupling constant $\ln \kappa$ is between 0.5 and 2.

Parameters	BaZr _{0.9} Y _{0.1} O _{3–δ}	BaZr _{0.8–x} Ce _x Y _{0.2} O _{3–δ} ($x = 0, 0.1, 0.2$)	BaCe _{0.8} Y _{0.2} O _{3–δ}
σ_{00} [K S cm ⁻¹]	1.12	0.0544	2.02×10^{-5}
T_{iso} [K]	596	498	297
$k_B T_{\text{iso}}$ [meV]	51.4	42.9	25.6
$h\nu$ [meV]	25.7–103	21.5–86	12.8–51.2
$\bar{\nu}$ [cm ⁻¹]	207–827	152–609	110–438

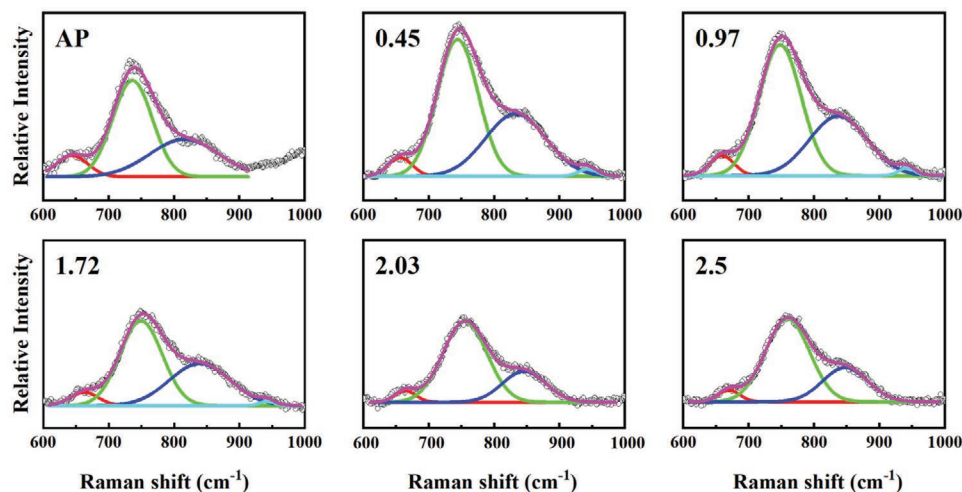


Figure 2. Raman peak fitting diagram ambient pressure (AP) to 2.5 GPa for the Zr–O stretching motion of $\text{BaZr}_{0.9}\text{Y}_{0.1}\text{O}_{3-\delta}$ from 600 to 1000 cm^{-1} . Black open circles: experimental data; purple line: cumulative fit; red line: ν_3 ; green line: ν_4 ; blue line: ν_5 . Three Gaussian functions were used in the peak fitting procedure.

ν_3 , ν_4 , and ν_5 were used for fitting the Zr–O stretching motion in the range between 600 and 1000 cm^{-1} . Two peaks named as ν_1 and ν_2 were used to fit the Ba–ZrO₆ stretching in the range between 100 and 120 cm^{-1} , and other two peaks named as τ_1 and τ_2 were used to fit the ZrO₆ torsion vibrations in the range between 150 and 350 cm^{-1} (Figures S3 and S4, Supporting Information).

Comparing the pressure-dependent changes in the Raman shifts, as shown in the slopes in Figure S5 (Supporting Information), it is clear that applied pressure has significantly affected the Zr–O stretching modes. To look for the correlations between these stretching and torsion Raman modes, and proton conductivity in BZY, in Figure 3, we plot the activation energy E_a , and prefactor σ_0 as a function of the Raman shifts under pressure. Upon pressurizing, the changes in ν_1 and ν_2 are not significant, therefore, E_a and σ_0 are virtually independent of the Ba–ZrO₆ stretching modes. For the ZrO₆ torsion (τ_1 and τ_2) and Zr–O stretching motions (ν_3 , ν_4 , and ν_5), the activation energy and prefactor increase linearly with increasing Raman frequency, but the slopes are different for each Raman mode. Both ZrO₆ torsion and Zr–O stretching belong to the motion within the Zr–O octahedron. Therefore, although each vibrational mode shows a different dependence

of E_a and σ_0 on Raman shift, we attribute the proton conductivity to the vibrational modes in the Zr–O octahedron, but not to the Ba–ZrO₆ stretching modes. This is in line with our previous findings on BCY.^[24,29]

The increase in prefactor is correlated to the increased phonon frequency by the attempt frequency of proton hopping. As demonstrated in our previous work,^[22] the attempt frequency scales linearly with the Arrhenius prefactor. The calculated attempt frequency is of the order of 10^{11} – 10^{12} Hz at ambient pressure,^[22] falling in a typical phonon frequency range (10^{12} Hz). Therefore, it is reasonable to at least consider that the attempt frequency for proton hopping originates from lattice vibration. At high pressure, the increase in activation energy would result in a decrease in vibration amplitude with increasing vibration frequency.^[36] In addition, as resolved by X-ray diffraction in Figure S6 (Supporting Information), at high pressure, a short Zr–O bond length hardens the phonon mode, which leads to a smaller displacement of oxygen ions. This reduces the phonon assistance for proton transfer. Pressure also reduces the size of the channel. These effects lead to a higher energy barrier for proton transport.^[22]

It may still be difficult to precisely identify the contribution of a specific vibration mode to the proton transport properties

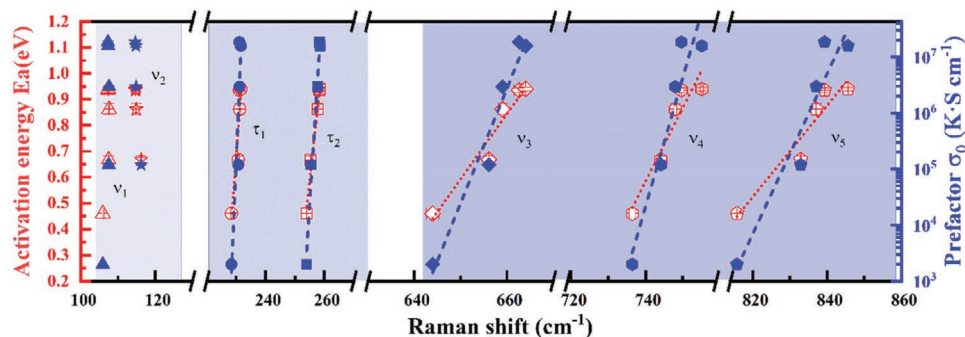


Figure 3. Correlation between activation energy (red open symbols), prefactor (blue closed symbols), and Raman bands for $\text{BaZr}_{0.9}\text{Y}_{0.1}\text{O}_{3-\delta}$. ν_1 and ν_2 : Ba–ZrO₆ stretching modes; τ_1 and τ_2 : ZrO₆ torsion motion; ν_3 , ν_4 , and ν_5 : Zr–O stretching motion.

such as E_a and σ_0 . We provide a qualitative discussion in the Supporting Information, see “Contribution of specific Raman modes,” from a differential perspective according to Figure 3. However, the present evidence provides hope that a more precise understanding of the vibration structure will hold the keys for unlocking the remaining secrets of proton migration in light of thermodynamics and cooperative behavior of protons with the lattice. From Figure 3, we are confident that the proton motion is dominated by vibrations within the Zr–O octahedron, which is known to provide pathways for proton hopping. Possibly, more element-specific vibration spectra such as known from nuclear resonant vibration spectroscopy could shed further light on this.^[37]

2.3. Correlation between Zr–O Stretch Vibration and Proton Conductivity

In perovskites, it is generally accepted that the ZrO₆ octahedron provides pathways for proton hopping,^[1,2,7,38,39] implying that only the vibrations of Zr and O atoms contribute to the proton transport. For instance, the O–M–O bending mode has been considered to provide proton transfer path.^[1,40–42] We have found that the Ce–O stretching mode best represents the proton transport in BCY oxide^[24] by analyzing the proton jump time applying Samgin’s proton polaron model.^[43] Through first-principles simulation, Toyoura found that in BaZrO₃, the Zr–O stretching modes contribute to proton hopping.^[44] Therefore, the O–M–O bending and M–O stretching modes have been considered to dominate the contribution of proton transport. In our high pressure Raman measurement, we did not observe prominent signal from bending modes due to their low Raman activity, therefore, in this work, we focus our discussion on the contribution from M–O stretching modes. Nevertheless, we cannot rule out the contribution from O–M–O bending modes on proton conductivity.

Here, we propose to consider the average frequency of ν_3 , ν_4 , and ν_5 , which we call “average Zr–O stretch vibration $\langle \nu \rangle$ ” in the following text, to describe the vibrational motion that controls the proton transport in perovskites. A justification for attributing the effect to these modes, based on the multiexcitation entropy model, is provided in the Supporting Information.

Figure 4a shows the average Zr–O stretch vibration as a function of pressure. We have transformed the ordinate of the Zr–O stretch vibration for BZY from wavenumbers, cm⁻¹, to

energy meV, in order to compare the Raman data with the excitation energy later. As the pressure increases, the average Zr–O stretch vibration $\langle \nu \rangle$ increases linearly by 9 cm⁻¹ GPa⁻¹ in wavenumbers, within the range pressure-dependent enhancement in Raman shift for ν_3 , ν_4 , and ν_5 in Figure S5 (Supporting Information). The increase of the Zr–O stretch vibration frequency indicates increased force constant under high pressure, that is, the lattice becomes “stiffer.” Such lattice hardening originates from the reduced Zr–O bond length under pressure, as shown in Figure S6b (Supporting Information). The relationship between Zr–O stretch vibration and proton conductivity is demonstrated in Figure 4b. With the increasing Zr–O stretch vibration, both the activation energy and the prefactor increase,^[22] consistent with their changes versus Raman shift shown in Figure 3.

3. Discussion

3.1. Correlation between Isokinetic Temperature, Vibrational Frequency, and Proton–Phonon Coupling

Following Equation (3), we show the Meyer–Neldel energy $k_B T_{\text{iso}}$ and T_{iso} as functions of the average M–O stretch vibration (M = Zr, Ce) for BZY, BaZr_{0.8-x}Ce_xY_{0.2}O_{3-δ} ($x = 0, 0.1, 0.2$) and BCY,^[29] in Figure 5. For the samples with Ce content greater than 0.1, the three modes ν_3 , ν_4 , and ν_5 merge into one band at 350 cm⁻¹,^[45] as shown in Figure S7 (Supporting Information). The vibration frequency of Ce–O stretch is much lower compared to Zr–O, because of larger Ce–O bond length, and heavier atomic weight of Ce. The isokinetic temperature increases with the increasing average M–O stretch vibration. We suggest that for perovskite-type proton conductors, higher isokinetic temperature is found in materials with higher average M–O stretch vibration. Therefore, the average M–O stretch vibration might be used as a simple descriptor to design new proton conductor materials with the desired isokinetic temperature.

Here, we have shown for analytical reasons how application of pressure can be used for the parameterization of the vibration energy. In technical applications, the use of epitaxial strain – compressive or tensile – may be a solution for tailoring the vibration structure and thus proton–phonon coupling for improved proton transport or any ion transport.

Figure 5 indicates that the average M–O stretch vibration is in the same order of magnitude as the Meyer–Neldel energy. In fact,

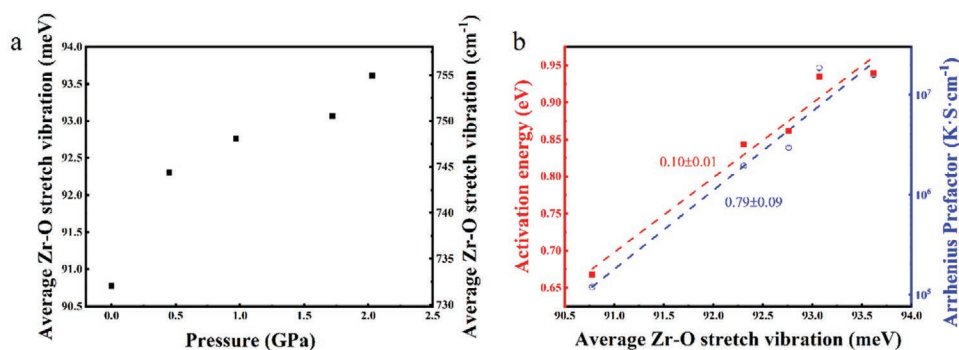


Figure 4. a) Average Zr–O stretch vibration $\langle \nu \rangle$ versus pressure for BaZr_{0.9}Y_{0.1}O_{3-δ}. b) Activation energy and prefactor of BaZr_{0.9}Y_{0.1}O_{3-δ} as a function of the average Zr–O stretch vibration $\langle \nu \rangle$.

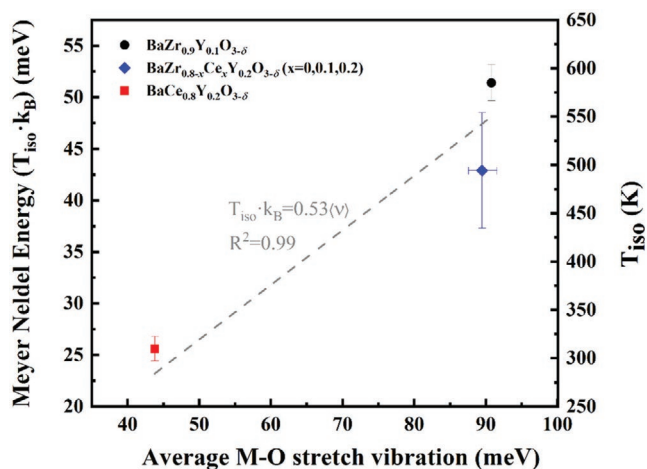


Figure 5. Correlation between Meyer–Neldel energy or isokinetic temperature and the average M–O stretch vibration $\langle \nu \rangle$ for $\text{BaZr}_{0.9}\text{Y}_{0.1}\text{O}_{3-\delta}$, $\text{BaZr}_{0.8-x}\text{Ce}_x\text{Y}_{0.2}\text{O}_{3-\delta}$ ($x=0, 0.1, 0.2$), and $\text{BaCe}_{0.8}\text{Y}_{0.2}\text{O}_{3-\delta}$. Dashed line represents fit according to Equation (3).

both T_{iso} and $\langle \nu \rangle$ of BCY are only 1/2 compared to those of BZY. Taking the average M–O stretch vibration to serve as the excitation energy in Equation (3), we calculated the corresponding coupling constant $\ln \kappa$, as listed in Table 2. For the three material systems investigated here, $\ln \kappa$ is about 2.0 ± 0.4 , indicating similar coupling energy between protons and the perovskite lattice. It has been suggested that the coupling constant is determined by phonon occupation statistics,^[46] which will provide a better understanding on the ion diffusion mechanism.

More data are required to confirm the correlations in Figure 5. We note that few data on isokinetic temperature are available, partly because changing the composition in proton conductors may also affect the microstructure, and proton concentration. Therefore, we propose that applying high pressure or variation of pressure in general be considered to be an effective approach to predict the isokinetic temperature for proton conductors. Similarly, the pressure-tuning approach has been proved as a rapid method to determine the Meyer–Neldel energy $k_B T_{\text{iso}}$ for lithium ionic conductors.^[35]

3.2. Tuning the Isokinetic Temperature According to MNR

In Figure 6a, we show the isokinetic prefactor σ_{00} as a function of the reciprocal of T_{iso} as obtained from Figure 1, and approximate the relationship between the two constants^[47]

$$\ln \sigma_{00} = \ln \sigma'_{00} - \frac{E_n}{k_B T_{\text{iso}}} \quad (5)$$

Table 2. The calculated average M–O stretch vibration $\langle \nu \rangle$ and coupling constant $\ln \kappa$ for $\text{BaZr}_{0.9}\text{Y}_{0.1}\text{O}_{3-\delta}$, $\text{BaZr}_{0.8-x}\text{Ce}_x\text{Y}_{0.2}\text{O}_{3-\delta}$ ($x=0, 0.1, 0.2$), and $\text{BaCe}_{0.8}\text{Y}_{0.2}\text{O}_{3-\delta}$.

$\text{BaZr}_{0.9}\text{Y}_{0.1}\text{O}_{3-\delta}$		$\text{BaZr}_{0.8-x}\text{Ce}_x\text{Y}_{0.2}\text{O}_{3-\delta}$ ($x=0, 0.1, 0.2$)		$\text{BaCe}_{0.8}\text{Y}_{0.2}\text{O}_{3-\delta}$	
$\langle \nu \rangle$ [meV]	$\ln \kappa$	$\langle \nu \rangle$ [meV]	$\ln \kappa$	$\langle \nu \rangle$ [meV]	$\ln \kappa$
90.8	1.77	86.7–91.3	2.30–2.42	43.8	1.60

where σ'_{00} and E_n are empirical constants that we will explain below. The proton conductivity in Figure 6 follows Equation (5) (shown as the solid fitting line), as observed previously in semiconductors,^[48] and in the proton conductivity in minerals.^[49] The fact that the proton conductivity is low, and that σ_{00} increases with T_{iso} , that is, it increases with the vibration frequency and decreases with $\ln \kappa$ (Figure 5), indicates that the conduction mechanism is polaronic,^[36] as we have proposed for perovskites, in general.^[14] We note that for temperatures higher than 800 K, one can see bending off of the conductivity curves in the Arrhenius plot around 800–900 K. This may arise from a decrease in the proton concentration with increasing temperature. Therefore, in Figure 6a, the apparent T_{iso} may deviate from the fitting line. This might suggest that there is also a limitation on the enhancement of proton conductivity by tuning T_{iso} . However, more data will be needed to reach a solid conclusion.

E_n is 0.66 ± 0.14 eV as calculated according to Equation (5). As shown in Figure 6b, for materials with activation energy $E_a < E_n$, large T_{iso} leads to high proton conductivity at low temperature, as indicated by the dashed line; whereas for materials with $E_a > E_n$, it is necessary to decrease T_{iso} to achieve high proton conductivity at the operating temperature (e.g., 800 K), as represented by the dotted line. Therefore, E_n is considered to be a critical energy to determine the strategy for improving the proton conductivity by tuning the isokinetic temperature. An example scenario is provided in Figure S8 (Supporting Information): for the bulk conductivity of BZY, the E_a is around 0.46 eV,^[50] smaller than the critical energy. When tuning T_{iso} from 596 to 1361 K,^[51] as achieved in BZY films with epitaxial strain, the proton conductivity is effectively enhanced.

From experiment, T_{iso} may be determined by computational simulations.^[52] For proton conductivity in perovskites, some other simple descriptors, such as ionic radii and basicity, are already known. Very likely, these descriptors turn out to be included in the concept of proton–phonon interaction. For example, basicity is related to polarizability,^[53] which has been shown to be closely related to phonons.^[21] Ionic radius is related to the bond length, which determines the vibration frequency.

4. Conclusion

We have confirmed the existence of a MNR between Arrhenius prefactor and activation energy for the proton conductivity in perovskite-type Y-doped BaMO_3 ($M = \text{Zr}$ or Ce), when the material structure is tuned by applying high pressure and by varying the Ce content. Since this behavior is likely to be caused by the free volume change in response to ion motion, it could be interesting to investigate the relation of MN behavior to activation volume, for an in-depth understanding of proton diffusion in perovskites. We have shown that when the isokinetic temperature calculated according to MNR is low, the adjustable range for proton conductivity is large. Therefore, the tunable range for proton conductivity can be adjusted by designing the material isokinetic temperature, breaking the limitation of MNR.

Following the multiexcitation entropy model, the isokinetic temperatures suggest that protons are excited by lattice phonons. The correlations between activation energy, prefactor, and

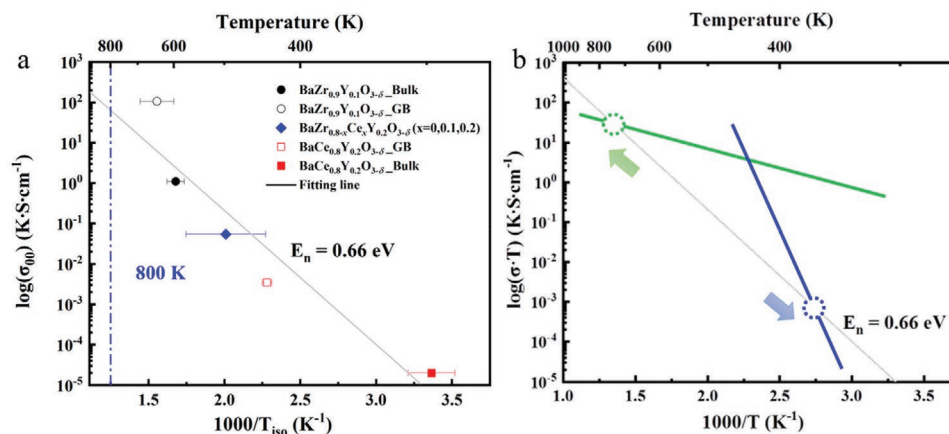


Figure 6. a). Correlation between isokinetic prefactor σ_{00} and isokinetic temperature T_{iso} and for $\text{BaZr}_{0.9}\text{Y}_{0.1}\text{O}_{3-\delta}$, $\text{BaZr}_{0.8-x}\text{Ce}_x\text{Y}_{0.2}\text{O}_{3-\delta}$ ($x=0, 0.1, 0.2$), and $\text{BaCe}_{0.8}\text{Y}_{0.2}\text{O}_{3-\delta}$. Solid line is the fit according to Equation (5) where $E_n = 0.66$ eV. The dashed-dotted line indicates the temperature of 800 K. b). Strategy to tune the T_{iso} . The green open circle represents the case when $E_a < E_n$, the blue open circle for $E_a > E_n$.

Raman shifts under high pressure emphasize the dominant contribution of vibrations within the M–O octahedron to the proton motion. We propose to use average M–O stretch vibration, as a lattice dynamics descriptor for BaMO_3 . Larger average M–O stretch vibration corresponds to lighter M atoms, with shorter M–O bond lengths and higher isokinetic temperatures. The relationship between isokinetic temperature, isokinetic prefactor σ_{00} , and average M–O stretch vibration reveals the polaronic nature of proton conductivity in perovskites.

Based on the understanding in this work, to design new perovskite materials with high proton conductivity, it is necessary to tune the material T_{iso} according to its activation energy. For proton conductors with $E_a < 0.66$ eV, to increase the isokinetic temperature, it is necessary to choose elements with weak proton–phonon coupling, as indicated in Equation (3). In addition, high T_{iso} is also correlated with large average M–O stretch vibration, which can be realized by choosing light atoms with small bond length. On the other hand, for proton conductors with $E_a > 0.66$ eV, a low isokinetic temperature offers high proton conductivity at the typical working temperature (e.g., 800 K). The design principle has potential to be more universally applied to other fast ionic conductors that follow MNR.

5. Experimental Section

A solid-state reaction method was used to prepare $\text{BaZr}_{0.9}\text{Y}_{0.1}\text{O}_{3-\delta}$.^[22] Oxide precursors including barium carbonate (General-Reagent, 99%), zirconium dioxide (Adamas, 99%), and yttrium oxide (Adamas, 99.99%) were dried and weighed according to their stoichiometric ratio. The precursor materials were ball-milled and calcined at 1200 °C for 10 h. The powder was pressed into pellets and sintered at 1720 °C for 24 h, and ground to powder again for high pressure measurements. The sample hydration was performed at 600 °C in a tubular furnace for 24 h in wet nitrogen flow (20 mL min⁻¹).

Raman spectroscopy was employed to study the lattice vibration under high pressure at room temperature, with the excitation laser of 532 nm and the power of 3 mW. High pressure was applied using a diamond anvil cell (DAC) with rhenium gaskets, and silicone oil as pressure transmit medium. The anvil culet size was 400 μm . The pressure was calibrated using the ruby luminescence method.^[54] High-pressure X-ray diffraction (XRD) was performed to investigate the structural evolution

under pressure, in angle-dispersive geometry at the beamline 15 U at the Shanghai Synchrotron Radiation Facility, using the same type of DAC as used for the Raman measurement. The X-ray wavelength was 0.6199 Å. Rietveld refinement was performed to determine the crystal lattice parameters using the software Match!3.^[55]

Supporting Information

Supporting Information is available from the Wiley Online Library or from the author.

Acknowledgements

Financial support from the National Natural Science Foundation of China (Grant No. 51802193 and 51772184) and the Swiss National Science Foundation (Grant No. 188588) are gratefully acknowledged. The high-pressure XRD was performed at the beamline 15 U at the Shanghai Synchrotron Radiation Facility. The authors thank Shou-Hang Bo and Hong Zhu (UM-SJTU Joint Institute) for valuable scientific discussions, and three anonymous reviewers for their comments and suggestions.

Conflict of Interest

The authors declare no conflict of interest.

Data Availability Statement

The data that support the findings of this study are available from the corresponding author upon reasonable request.

Keywords

activation energy, ceramic proton conductors, isokinetic temperature, lattice dynamics, Meyer–Neldel rule, proton conductivity

Received: September 21, 2021

Revised: December 2, 2021

Published online: December 22, 2021

- [1] K. D. Kreuer, *Annu. Rev. Mater. Res.* **2003**, *33*, 333.
- [2] E. Fabbri, D. Pergolesi, E. Traversa, *Chem. Soc. Rev.* **2010**, *39*, 4355.
- [3] C. Duan, J. Tong, M. Shang, S. Nikodemski, M. Sanders, S. Ricote, A. Almansoori, R. O'Hayre, *Science* **2015**, *349*, 1321.
- [4] S. Hossain, A. M. Abdalla, S. N. B. Jamain, J. H. Zaini, A. K. Azad, *Renewable Sustainable Energy Rev.* **2017**, *79*, 750.
- [5] C. Q. Xia, J. Peng, S. Ponce, J. B. Patel, A. D. Wright, T. W. Crothers, M. Uller Rothmann, J. Borchert, R. L. Milot, H. Kraus, Q. Lin, F. Giustino, L. M. Herz, M. B. Johnston, *J. Phys. Chem. Lett.* **2021**, *12*, 3607.
- [6] W. Zhang, Y. H. Hu, *Energy Sci. Eng.* **2021**, *9*, 984.
- [7] D. Han, X. Liu, T. S. Bjørheim, T. Uda, *Adv. Energy Mater.* **2021**, *11*, 2003149.
- [8] E. Gilardi, E. Fabbri, L. Bi, J. L. M. Rupp, T. Lippert, D. Pergolesi, E. Traversa, *J. Phys. Chem. C* **2017**, *121*, 9739.
- [9] K. Toyoura, T. Fujii, N. Hatada, D. Han, T. Uda, *J. Phys. Chem. C* **2019**, *123*, 26823.
- [10] Y. Yamazaki, F. Blanc, Y. Okuyama, L. Buannic, J. C. Lucio-Vega, C. P. Grey, S. M. Haile, *Nat. Mater.* **2013**, *12*, 647.
- [11] D. Z. Sahraoui, T. Mineva, *Solid State Ionics* **2013**, *253*, 195.
- [12] T. Norby, M. Wideroe, R. Glockner, Y. Larring, *Dalton Trans.* **2004**, 3012.
- [13] D. Noferini, B. Frick, M. M. Koza, M. Karlsson, *J. Mater. Chem. A* **2018**, *6*, 7538.
- [14] A. Braun, Q. Chen, A. Yelon, *Chimia* **2019**, *73*, 936.
- [15] W. Meyer, H. Neldel, *Phys. Z.* **1937**, *38*, 1014.
- [16] W. Meyer, H. Neldel, *Z. Tech. Phys.* **1937**, *18*, 588.
- [17] F. H. Constable, *Proc. R. Soc. A* **1925**, *108*, 355.
- [18] A. G. Jones, *Geochem., Geophys., Geosyst.* **2014**, *15*, 337.
- [19] A. Yelon, B. Movaghar, *Phys. Rev. Lett.* **1990**, *65*, 618.
- [20] A. Yelon, B. Movaghar, R. Crandall, *Rep. Prog. Phys.* **2006**, *69*, 1145.
- [21] S. Muy, R. Schlem, Y. Shao-Horn, W. G. Zeier, *Adv. Energy Mater.* **2021**, *11*, 2002787.
- [22] Z. Fan, N. Li, P. Du, W. Yang, Q. Chen, *J. Phys. Chem. C* **2020**, *124*, 22376.
- [23] P. Du, Q. Chen, Z. Fan, H. Pan, F. G. Haibach, M. A. Gomez, A. Braun, *Commun. Phys.* **2020**, *3*, 200.
- [24] A. Braun, Q. Chen, *Nat. Commun.* **2017**, *8*, 15830.
- [25] S. Muy, J. Voss, R. Schlem, R. Koerver, S. J. Sedlmaier, F. Maglia, P. Lamp, W. G. Zeier, Y. Shao-Horn, *iScience* **2019**, *16*, 270.
- [26] S. Muy, J. C. Bachman, L. Giordano, H.-H. Chang, D. L. Abernathy, D. Bansal, O. Delaire, S. Hori, R. Kanno, F. Maglia, S. Lupart, P. Lamp, Y. Shao-Horn, *Energy Environ. Sci.* **2018**, *11*, 850.
- [27] Y. Gao, A. M. Nolan, P. Du, Y. Wu, C. Yang, Q. Chen, Y. Mo, S. H. Bo, *Chem. Rev.* **2020**, *120*, 5954.
- [28] M. A. Kraft, S. Ohno, T. Zinkevich, R. Koerver, S. P. Culver, T. Fuchs, A. Senyshyn, S. Indris, B. J. Morgan, W. G. Zeier, *J. Am. Chem. Soc.* **2018**, *140*, 16330.
- [29] Q. Chen, T.-W. Huang, M. Baldini, A. Hushur, V. Pomjakushin, S. Clark, W. L. Mao, M. H. Manghnani, A. Braun, T. Graule, *J. Phys. Chem. C* **2011**, *115*, 24021.
- [30] Q. Chen, A. Braun, S. Yoon, N. Bagdassarov, T. Graule, *J. Eur. Ceram. Soc.* **2011**, *31*, 2657.
- [31] Q. Chen, A. Braun, A. Ovalle, C. D. Savaniu, T. Graule, N. Bagdassarov, *Appl. Phys. Lett.* **2010**, *97*, 333.
- [32] Q. Chen, *Doctoral Thesis*, ETH Zurich **2012**.
- [33] D. Han, K. Goto, M. Majima, T. Uda, *ChemSusChem* **2021**, *14*, 614.
- [34] T. Famprikis, O. U. Kudu, J. A. Dawson, P. Canepa, F. Fauth, E. Suard, M. Zbiri, D. Dambournet, O. J. Borkiewicz, H. Bouyanff, S. P. Emge, S. Cretu, J. N. Chotard, C. P. Grey, W. G. Zeier, M. S. Islam, C. Masquelier, *J. Am. Chem. Soc.* **2020**, *142*, 18422.
- [35] Y. Gao, N. Li, Y. Wu, W. Yang, S.-H. Bo, *Adv. Energy Mater.* **2021**, *11*, 2100325.
- [36] K. Wakamura, *Solid State Ionics* **2009**, *180*, 1343.
- [37] H. Wang, A. Braun, S. P. Cramer, L. B. Gee, Y. Yoda, *Crystals* **2021**, *11*, 909.
- [38] L. Malavasi, C. A. Fisher, M. S. Islam, *Chem. Soc. Rev.* **2010**, *39*, 4370.
- [39] F. M. Draber, C. Ader, J. P. Arnold, S. Eisele, S. Grieshammer, S. Yamaguchi, M. Martin, *Nat. Mater.* **2020**, *19*, 338.
- [40] Y. Jing, N. R. Aluru, *J. Power Sources* **2020**, *445*, 227327.
- [41] K.-D. Kreuer, A. Fuchs, J. Maier, *Solid State Ionics* **1995**, *77*, 157.
- [42] N. Kuwata, N. Sata, T. Tsurui, H. Yugami, *Jpn. J. Appl. Phys.* **2005**, *44*, 8613.
- [43] A. L. Samgin, *Solid State Ionics* **2000**, *136–137*, 291.
- [44] K. Toyoura, N. S. G. Found, *Mater. Sci. Eng., R* **2020**, *38*.
- [45] C. Chemarin, N. Rosman, T. Pagnier, G. Lucazeau, *J. Solid State Chem.* **2000**, *149*, 298.
- [46] T. Bernges, R. Hanus, B. Wankmiller, K. Imasato, S. Lin, M. Ghidui, M. Gerlitz, M. Peterlechner, S. Graham, G. Hautier, (Preprint) arXiv:10.33774, v1, submitted: Sept **2021**.
- [47] A. Yelon, *MRS Adv.* **2017**, *2*, 425.
- [48] F. Abdel-Wahab, A. Yelon, *J. Appl. Phys.* **2013**, *114*, 023707.
- [49] A. G. Jones, *Geochem., Geophys., Geosyst.* **2014**, *15*, 2616.
- [50] S. Duval, P. Holtappels, U. Vogt, U. Stimming, T. Graule, *Fuel Cells* **2009**, *9*, 613.
- [51] A. Fluri, A. Marcolongo, V. Roddatis, A. Wokaun, D. Pergolesi, N. Marzari, T. Lippert, *Adv. Sci.* **2017**, *4*, 1700467.
- [52] X. Li, L. Zhang, Z. Tang, M. Liu, *J. Phys. Chem. C* **2019**, *123*, 25611.
- [53] V. Dimitrov, T. Komatsu, *J. Solid State Chem.* **2012**, *196*, 574.
- [54] H. K. Mao, P. M. Bell, *Carnegie Inst. Washington, Year Book* **1978**, *77*, 904.
- [55] H. Putz, K. Brandenburg, *Match! - Phase Analysis using Powder Diffraction*, <https://www.crystalimpact.de/match> (accessed: August 2021).